THE ASTROPHYSICAL JOURNAL, 494:700–714, 1998 February 20

BASAL HEATING IN MAIN-SEQUENCE STARS AND GIANTS: RESULTS FROM MONOCHROMATIC ACOUSTIC WAVE MODELS

BERND BUCHHOLZ AND PETER ULMSCHNEIDER
Institut für Theoretische Astrophysik, Universität Heidelberg, Tiergartenstraße 15, D-69121 Heidelberg, Germany;
ulm@ita.uni-heidelberg.de

AND

MANFRED CUNTZ
Center for Space Plasma, Aeronomy, and Astrophysics Research (CSPAAR), University of Alabama in Huntsville,
Huntsville, AL 35899; cuntzm@cspar.uah.edu
Received 1997 May 5; accepted 1997 September 29

ABSTRACT

We calculate time-dependent models of acoustically heated chromospheres for main-sequence stars between spectral type F0 V and M0 V and for two giants of spectral type K0 III and K5 III assuming monochromatic waves. The hydrodynamic equations are solved together with the radiative transfer and statistical equilibrium equations to investigate the propagation of acoustic waves into the chromospheric regions. The emergent radiation in Mg II $h + k$ and Ca II H + K is calculated and compared with observations. We find good agreement, over nearly 2 orders of magnitude, between the time-averaged emission in these lines and the observed basal flux emission, which had been suspected to be due to nonmagnetic (i.e., acoustic) heating operating in all late-type stars. The height dependence of the acoustic energy flux can be explained by the limiting strength property of the acoustic shocks and is consistent with that found in models of quiet solar regions. We also confirm the validity of the Ayres scaling law, which has originally been derived for semiempirical chromosphere models and is thus independent of assumptions about the chromospheric heating mechanism. Our results strongly support the idea that the "basal heating" of chromospheres of late-type stars as revealed by the frequency-integrated Mg II and Ca II line emission is fully attributable to the dissipation of acoustic wave energy.

Subject headings: hydrodynamics — line: formation — shock waves — stars: activity — stars: chromospheres — stars: late-type

1. INTRODUCTION

An outstanding problem in stellar astrophysics concerns the identification of the processes responsible for heating stellar chromospheres and coronae and for driving stellar winds. During the past 20 years, major advances have been made, in part owing to different types of observations obtained by *IUE*, *ROSAT*, and *HST*-GHRS, to solar observations, and to sophisticated theoretical modeling (see, e.g., Linsky 1991; Pallavicini 1992; Ulmschneider 1990, 1993; Cuntz 1996; among others). Based on these results, it has been concluded that two different types of mechanisms for chromospheric heating exist, which can broadly be classified as magnetic heating and acoustic heating. These heating processes are expected to have a different impact in stars of different effective temperature, surface gravity, and rotation rate and to change dramatically during the course of stellar evolution. For recent reviews on proposed heating mechanisms, see, e.g., Narain & Ulmschneider (1990, 1996).

Schrijver (1987) and Rutten et al. (1991) have provided major contributions to the disentanglement of the relative importance of magnetic and acoustic heating in chromospheres of late-type stars. They argued that the emission flux of each chromospheric line may consist of two components: a "basal" flux Φ, which is independent of the stellar rotation rate, and a "magnetic" flux, which depends on rotation and (by implication) on age. In the case of single stars, fast rotation usually increases the chromospheric line emission considerably. Schrijver and Rutten et al. identified the basal flux limits of Mg II and Ca II as an intrinsic property of the stars, which remain unaffected by detection limits. Schrijver (1987) and Schrijver, Dobson, & Radnick (1989) argued that since the chromospheric basal flux limits of specific lines are independent of the stellar rotation rate, they can best be attributed to pure acoustic heating. Acoustic heating remains essentially unaffected by stellar rotation and depends only on the stellar effective temperature and gravity and in a very limited sense also on the metal abundances. Stars that only have the basal flux components are usually referred to as *chromospheric basal flux stars*. The latter authors presented a detailed analysis for the Mount Wilson Ca II H and K fluxes of cool dwarfs containing evidence for the existence of magnetic, basal, and radiative-equilibrium components in these lines. Note that Middelkoop (1982), who analyzed the Ca II H and K lines of a total of 335 evolved stars, mostly giants, already provided preliminary evidence for the existence of basal limits in the fluxes of chromospheric emission lines. The most recent status of this type of work has been outlined in the review of Schrijver (1995).

There are also other observational indications that suggest the separation into two distinct chromospheric heating components. One of these is the spread in chromospheric emission in samples of stars of a given spectral type and luminosity class. Magnetic heating, due to the variation of the stellar rotation rates, generates a wide spread of chromospheric emission fluxes for the same type of stars. Acoustic heating, however, which does not depend on stellar rotation, gives always roughly the same emission flux for stars of the same effective temperature and gravity, which thus leads to no or only a narrow spread in chromospheric emission. As a consequence, a wide spread of the chromospheric emission is evidence that magnetic heating

dominates. The decrease of this spread in chromospheric activity with decreasing $B-V$, toward F stars, is well documented (Rutten 1987, Fig. 1; Walter & Schrijver 1987, Fig. 1). This can be explained by the two-component heating picture in a straightforward manner. The acoustic heating component, as derived from acoustic wave generation calculations, increases strongly toward decreasing $B-V$ and increasingly overwhelms the magnetic heating component. Here a strong nonspread emission component adds to a wide-spread emission component and thereby reduces the resulting spread. Therefore, the acoustic heating component is expected to dominate in many inactive cool stars, including F stars. That acoustic wave heating is consistent with the basal flux emission of M dwarf stars has also been found by Mathioudakis & Doyle (1992).

Links to theoretical studies of angular momentum evolution have been discussed by Gray (1991), Schrijver (1993), Schrijver & Pols (1993), and Charbonneau, Schrijver, & MacGregor (1997), among others. These studies show that when solar-type stars evolve apart from the main sequence, their angular momentum subsides, in part owing to the increase in the moment of inertia caused by changes in the internal mass distribution and in part owing to magnetic braking resulting from the onset of massive stellar winds. It has therefore been argued that the dominant chromospheric heating mechanism in single inactive late-type (super-) giants might be essentially acoustic rather than magnetic in nature. This result has found support in further studies of Pasquini, Pallavicini, & Pakull (1988), Dupree, Hartmann, & Smith (1990), Judge & Stencel (1991), Strassmeier et al. (1994), and Peterson & Schrijver (1997), which demonstrate the reality of empirically deduced basal flux limits. Judge & Stencel (1991) and Cuntz et al. (1996) have studied the Mg II basal flux limits at low effective temperatures to evaluate the activity level of noncoronal K giants. Peterson & Schrijver analyzed Mg II spectra of nine metal-poor solar-type stars, some believed to be among the oldest stars known. They found that in all stars the level of Mg II emission is commensurate with the basal flux limit, which is further support for the acoustic heating picture.

These results show that the dominant heating mechanism in chromospheric basal flux stars may be acoustic rather than magnetic. An alternative, or perhaps supplementary, explanation of basal heating is that it may be caused by heating due to intrinsically weak magnetic fields generated by the dynamo mechanism working at a very low stellar rotation rate or by convective turbulence of the partly ionized matter. Furthermore, those magnetic fields could also be a leftover from an earlier evolutionary status of the star. These types of explanations, however, have not gained support by detailed model calculations. On the other hand, it should be noted that in case of main-sequence stars, magnetic surface structures must also be present as they are necessary to heat the coronae. In case of inactive late-type giants, indirect evidence for the presence of magnetic fields exists, as current acoustic shock wave models are found to be unable to explain the size of observed mass-loss rates (Hartmann & MacGregor 1980; Cuntz 1990; Sutmann & Cuntz 1995) and the magnitude of chromospheric turbulence (Judge & Cuntz 1993). On the other hand, it is fully legitimate to calculate acoustic heating models for these stars, as they possess sizable convection zones, which give rise to acoustic energy generation.

It is the purpose of this paper to calculate theoretical heating models for cool star chromospheres based on acoustic energy dissipation. We focus on main-sequence stars of spectral type F0 V–M0 V and on giant stars of spectral type K0 III–K5 III and simulate the atmospheric properties of these stars, notably the emerging radiation in Mg II and Ca II. These results are then compared with observations. Our paper is structured as follows: In § 2, we discuss our method and model assumptions. Section 3 gives specific results for chromospheric heating models of main-sequence stars and giants, including the calculation of Mg II and Ca II emission lines. In § 4, we evaluate the position of the theoretical Mg II and Ca II basal flux limits in relationship to observational data. Conclusions are given in § 5.

2. METHOD AND MODEL ASSUMPTIONS

The computation of acoustic waves has been discussed in previous work by us (Ulmschneider et al. 1977; Ulmschneider, Muchmore, & Kalkofen 1987; Schmitz, Ulmschneider, & Kalkofen 1985; Rammacher & Ulmschneider 1992) and therefore does not need to be described again in detail. The basic features of these computations include the following:

1. We adopt solutions of the one-dimensional hydrodynamic equations, which consist of the continuity equation, the momentum equation, and the energy equation. The solutions are obtained using the method of characteristics.
2. At the bottom of the atmosphere, we introduce sinusoidal acoustic waves generated by a piston. The waves are followed to the point of shock formation and beyond.
3. The shocks are treated as discontinuities and are allowed to grow to arbitrary strength. Since we utilize the method of characteristics, there is no need to use numerical viscosity for the treatment of the shocks. The shocks are also permitted to merge with each other.
4. At the top of the atmosphere, we use a transmitting boundary condition. Details about the implementation of the transmitting boundary condition into the method of characteristics have been described by Ulmschneider (1986).
5. Radiative energy losses (and gains) are described by solving the radiation transfer equations in the H^- continuum as well as the Mg II k and H Lyα lines (as representative chromospheric emitters, assuming complete redistribution [CRD]). The radiative transfer equations are solved together with the statistical equilibrium equations for NLTE populations.
6. H^- (bound-free and free-free) is treated in NLTE as in Vernazza, Avrett, & Loeser (1981) except for the use of an electron density table computed with Kurucz's ATLAS program using LTE.
7. The Mg II k and Lyα line cooling rates are been computed using the operator splitting method (Buchholz et al. 1994), which is more accurate and faster than the modified core-saturation method previously used by Rammacher & Ulmschneider (1992).
8. We do not include molecules such as CO. Therefore, we do not consider the possible influence of thermal bifurcation and thermal instabilities in our models.

It should be particularly noted that we have not treated the ionization of hydrogen consistently together with the equations of hydrodynamics. Specifically, we have not included the hydrogen ionization energy in the energy equation. Time-dependent ionization and recombination effects

of hydrogen are also important (see, e.g., Kneer 1980; Carlsson & Stein 1992, 1995) but have not been included either. Interestingly, both approximations are expected to change the thermal structure of the atmospheres in opposite directions: ignoring the ionization energy of hydrogen in the energy equation produces an atmosphere that is definitely too hot, while including this term but omitting the advective term as well as the time-derivative term in the statistical hydrogen rate equations produces an atmosphere that is too cool, particularly in regions behind shocks. Thus, our present treatment represents a compromise. Nevertheless, it is our plan to include both effects in our radiation-hydrodynamics code, which is currently under development (Cuntz & Höflich 1998). For our acoustic wave calculations, we also need starting atmospheres in radiative equilibrium because otherwise the atmospheres, after starting the time-dependent treatment, would show motions even in the absence of waves. To generate starting atmospheres, we use the same equations as in the time-dependent hydrodynamic code, the same height grid, and also employ the same radiation treatment. The starting models are then constructed by using the usual temperature and flux correction procedures as discussed by Cuntz, Rammacher, & Ulmschneider (1994).

The energy flux and spectrum of acoustic waves generated in the convection zone of stars other than the Sun cannot be observed but must be computed theoretically. The most advanced theoretical method to compute acoustic wave generation from the turbulent motions in stellar convection zones is the Lighthill-Stein theory. This theory and its background have recently been rediscussed by Musielak et al. (1994) and Ulmschneider, Theurer, & Musielak (1996). It was found that the older version of Stein's theory, Bohn (1981, 1984), gives basically realistic results if an unrealistically low mixing-length parameter of $\alpha = 1.0$ is adopted as it has been done in the present work. In that case, the wave energy fluxes are found to be commensurate with the results of Ulmschneider et al. (1996) obtained using a mixing-length parameter of $\alpha = 2.0$. In this case, the differences are mostly smaller than a factor of 1.5, except for the M0 V star for which the acoustic energy fluxes given by Bohn are overestimated by more than a factor of 10. For main-sequence stars between F5 V and K0 V, the results are virtually identical.

Note that relatively large mixing-length parameters are now strongly preferred in the literature. Nordlund & Dravins (1990) who presented three-dimensional convective models combined with three-dimensional nongray radiative transfer for a set of main-sequence stars and subgiants argued that α might be $\simeq 1.5$ (or somewhat larger). Values of α between 1.7 and 2.0 are also preferred by Kumar (1994) and Musielak et al. (1994). A value of $\alpha = 2.0$ is also indicated by a comparison of the peak value of the convective velocity in mixing-length calculations with that in time-dependent hydrodynamic convection simulations (Steffen 1992), as well as by a careful fitting of evolutionary tracks of solar-type stars with the mass, luminosity, and age of ζ Aurigae system primaries (Schröder, Pols, & Eggleton 1997).

A further reason why Bohn's results are still useful is that our wave computations are based on monochromatic waves. In this case, a limiting strength for the shocks is achieved, which means that the density, pressure, velocity, and temperature jumps across the shocks as well as the energy dissipation rate are largely independent of the initial acoustic energy flux. This situation, however, is changed as soon as acoustic frequency spectra are adopted. Bohn computed a large number of acoustic wave spectra of stars in the H-R diagram, shown also by Ulmschneider (1991). These spectra are very similar in shape to the recent solar spectra, with a similarly smooth and pronounced peak near $\omega = 5\omega_A$. As we want to use monochromatic acoustic waves in our time-dependent wave calculations, we thus adopt wave periods of $P = P_A/5$ for our model atmospheres, where $P_A = 4\pi c/\gamma g = 2\pi/\omega_A$ is the acoustic cutoff period. This choice can be justified by results from Sutmann & Ulmschneider (1995b), who used different kinds of frequency spectra to examine acoustic wave propagation in the solar atmosphere for adiabatic cases. They found that the average shock strengths obtained are in good agreement with those from calculations with purely monochromatic waves with a period of $P = 0.2P_A$.

For our calculations of the NLTE line emission, we assume two-level atoms while using the line data of Kalkofen, Ulmschneider, & Schmitz (1984). The background continua were computed using the ATLAS code of Kurucz. As already discussed in a previous paper (Ulmschneider et al. 1987), the task of solving the energy equation in an acoustic wave calculation requires the computation of the entire chromospheric cooling function which consists of many lines and continua. Because of the limited computer power available, it is not yet feasible to simultaneously treat many lines and continua with our time-dependent method. We therefore rely on the following approach: together with the H^- losses, we treat only the Mg II k and H Lyα line cooling, assuming CRD. These computations were performed with the operator splitting method given by Buchholz et al. (1994), which is fast and thus well suited for time-dependent applications. The use of CRD leads to about a factor of 10 more line cooling than when using partial redistribution (PRD) (Hünerth & Ulmschneider 1995) and thus very crudely incorporates the bulk of the chromospheric line emitters. This procedure (without Lyα) has been tested (Ulmschneider et al. 1987) for the Sun by comparison with the total cooling rate of chromosphere model C of Vernazza et al. (1981). The additional Lyα losses contribute only at great height, where the Mg line cooling becomes weak. However, Lyα cooling is nevertheless important in our present models as it contributes to the damping of the large pulsational oscillations during the switch-on phase of the wave computations, which would otherwise develop into strong shocks. The treatment of Lyα is also a potential source of systematic errors, particularly in the outermost regions of the models, but appears to be reasonable, since it does not affect the regions of Mg II line cooling very much.

Nevertheless, we note that the emission-line fluxes and profiles can be computed properly only when effects due to PRD are taken into account (see, e.g., Ayres & Linsky 1976; Drake & Linsky 1983; Judge 1990). This result is particularly relevant when emission fluxes from individual lines are studied. We thus follow this approach when we compare the theoretical line fluxes of Mg II and Ca II with observations (see § 4). For this we utilize the new PRD operator splitting method by Ulmschneider (1994). The redistribution is computed using the R II function of Gouttebroze (1986) and the data of the respective atomic model. This procedure is consistently used for calculating Mg II and Ca II line fluxes and line profiles of our target stars for distinct time steps of the wave models.

3. RESULTS AND DISCUSSION

3.1. *Theoretical Chromosphere Models*

We now discuss our hydrodynamic models in detail. The wave motion is initiated by means of a piston. This produces acoustic waves that heat up the chromosphere by forming shocks. The sample of main-sequence stars in this investigation ranges from spectral type F5 V to M0 V (see Table 1). We use the initial acoustic energy fluxes of Bohn (1981, 1984) including the corresponding wave periods derived from his spectra. Figure 1 shows a snapshot of the wave calculation for the F5 V star after 1123 seconds. The adopted wave period has been 50 s, and about 22 wave periods have already entered the atmosphere. The energy dissipation of the shocks has increased the temperature in the outer parts of the atmosphere. The shock formation height is at a mass column density of about $m = 0.1$ g cm^{-2}, which corresponds to a geometrical height of about 500 km above the top of the convection zone. Both the temperature and gas velocity distributions show a distortion of the wave profile with increasing height, starting from a sinusoidal shape to a sawtooth wave form typical for fully developed shocks, a behavior already found in earlier studies (see, e.g., Ulmschneider et al. 1987). The velocity jumps at the shocks quickly grow from the point of shock formation to about 6 km s^{-1} and remain almost constant with height although the density decreases several orders of magnitude.

This behavior is due to the *limiting shock strength* behavior found for monochromatic waves. The strength of a shock can be described by the shock strength parameter η, which is defined as

$$\eta = \frac{\rho_2 - \rho_1}{\rho_1}\,, \tag{1}$$

where ρ_1 and ρ_2 denote the density in front and behind the shock, respectively. The shock strength can also be described by the shock Mach number M_s, given by $M_s = (U_s - u_1)/c_1$. Here U_s denotes the shock speed, whereas u_1 and c_1 are the flow and sound speed, respectively, in front of the shock. In case of an ideal gas with $\gamma = 5/3$ being the ratio of the specific heats, the density jump across the shock is given by

$$\frac{\rho_2}{\rho_1} = \frac{(\gamma + 1)M_s^2}{(\gamma - 1)M_s^2 + 2}\,, \tag{2}$$

which allows us to calculate η. Similar equations hold for the jump of velocity, pressure, and temperature (see, e.g., Landau & Lifshitz 1975). In an isothermal, nonionizing atmosphere, it is known that shocks of relatively low strength in the absence of significant radiative damping reach a limiting strength $\eta^{\rm lim}$, which is independent of the initial wave energy flux and only dependent on the wave period (Brinkley & Kirkwood 1947; Ulmschneider 1970). For an atmosphere with gravity g, this limiting strength is given by

$$\eta^{\rm lim} = \frac{\gamma g P}{(\gamma + 1)c_s}\,. \tag{3}$$

Here P denotes the period of the wave, and c_s denotes the sound speed.

In the context of our investigation, we consider only waves with periods shorter than the acoustic cutoff period P_A, given by $P_A = 4\pi c_s/\gamma g$. As the actual wave period is given by $P = fP_A$ with $f < 1$, the resulting shock strength is then $\eta^{\rm lim} = 4.71f$. For our models we selected $f = 0.2$ (see § 2), which results in $\eta^{\rm lim} = 0.942$. The shock strengths in our time-dependent computations are influenced by radiative damping and can reach high values, where the small-amplitude assumption used for the derivation of the limiting strength formula no longer applies. The limiting shock strength behavior itself still persists (Cuntz & Ulmschneider 1988), and usually $\eta^{\rm lim}$ from equation (3) pre-

TABLE 1

PARAMETERS OF THE STARS AND HYDRODYNAMIC MODELS

Star	$B-V$	$T_{\rm eff}$ (K)	log g (cgs)	log F_M (cgs)	P (s)
F0 V	0.30	7200	4.34	9.08	55
F5 V	0.44	6440	4.34	8.82	50
G0 V	0.58	6030	4.39	8.51	45
G5 V	0.68	5770	4.49	8.27	40
K0 V	0.81	5250	4.49	7.88	35
K5 V	1.15	4350	4.54	7.06	26
M0 V	1.40	3850	4.59	6.26	22
K0 III.....	1.00	4750	2.13	8.60	3500
K5 III.....	1.50	3950	1.74	8.00	8000

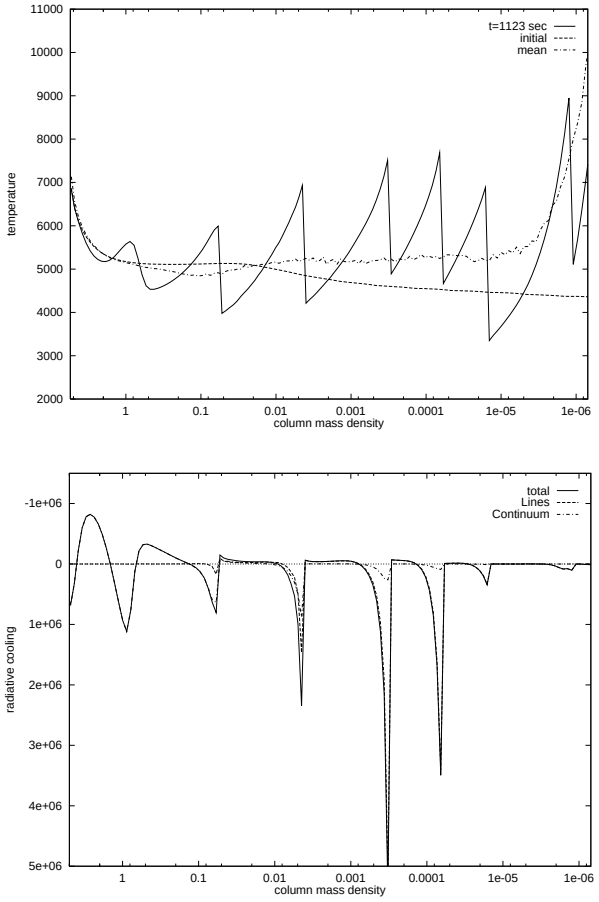

FIG. 1.—Snapshots showing atmospheric quantities for the F5 V star as function of the mass column density (g cm^{-2}) after $t = 1123$ s. The upper figure depicts various temperatures (K), which are the current temperature (*solid line*), the initial temperature (*dashed line*), and the mean (i.e., time-averaged) temperature (*dashed-dotted line*). The lower figure depicts the radiative damping function D (ergs g^{-1} K^{-1} s^{-1}) (*solid line*) consisting of the contribution of the Mg II k line (*dashed line*) and the H$^-$ continuum (*dashed-dotted line*).

dicts the value of η quite well, except for relatively large wave periods. For the calculations for the F5 V star, we find a density ratio at the shocks of $\rho_2/\rho_1 = 1.86$, which implies a shock strength parameter $\eta^{\rm lim} = 0.86$, which is 9% smaller than the value given by equation (3).

While the shock heating of short period waves with $P = 0.2P_A$ is sufficient to balance the chromospheric radiation losses, this type of wave is not able to produce significant stellar wind flows (see, e.g., Cuntz 1990), as they do not carry enough energy to a Parker-type critical point. In addition to the acoustic shock wave heating, the radiative energy losses are crucial for determining the atmospheric temperature structure, which in turn is relevant for the formation of chromospheric emission lines. Based on Figure 1, we identify several regions of the atmosphere in which different contributors to the radiative energy damping of the waves are most important. From the bottom of the atmosphere up to a mass column density $m = 0.09$ g cm^{-2}, which corresponds to a geometrical height of 700 km, the H^- continuum radiation dominates the radiative damping function $D = ds/dt|_R$ (with s being the specific entropy), while the contributions from the spectral lines are negligible. Then follows a region in which the lines and the H^- continuum are about equally important. In the overlying atmosphere, starting at $m = 0.0001$ g cm^{-2} in the F5 V star atmosphere model, only line radiation is important. Note that as soon as the shock is fully developed, the radiative damping is almost entirely concentrated in the hot postshock regions. In these postshock regions, the temperatures exceed $T \simeq 5800$ K and are often as high as 7000 K. In the top part of the atmosphere, the opacity in the lines and in the H^- continuum is so small that the waves behave quasi-adiabatically. This leads eventually to unbalanced heating and the formation of a transition layer–type structure. The formation of such a transition layer–type temperature rise is inevitable as from equation (10) (below) we see that the heating rate decreases with ρ while the radiative emission, as usual, decays comparable to or faster than a ρ^2-dependence.

It should also be noted that for the F5 V star, the point of shock formation is found inside the radiative damping zone where H^- dominates. This zone extending from the bottom of the atmosphere up to $m = m_L \simeq 0.2$ g cm^{-2} is defined by $t_R < P$, where

$$t_R = \frac{c_v}{16\sigma\kappa T^3} \tag{4}$$

is the radiative damping time (Spiegel 1957; see also Ulmschneider 1988; Schmitz 1990). Here c_v is the specific heat per gram at constant volume, σ is the Stefan-Boltzmann constant, κ is the Rosseland mean opacity per gram, and T is the temperature.

This equation can be utilized to estimate t_R, which can then be set in relation to the wave period P. It is found that when $t_R < P$, the waves lose their energy primarily by radiation damping instead of shock dissipation. Moreover, in the radiation damping zone the shocks are prevented from growing to sawtooth shape until they reach the limit m_L, which is the region in which H^- radiation is essentially negligible. Zhugzhda, Dzhalilov, & Staude (1993) have meanwhile improved equation (4) by avoiding the use of the Rosseland mean opacity. Their results differ from those of equation (4) by less than 10%.

Some of the atmospheric properties change, when the cooler stars of our sample are considered. Figure 2 shows the temperature structure of an acoustically heated chromosphere model of a K5 V star after 1286 s. The wave period used for this star is $P = 26$ s, and 50 wave periods have already entered the atmosphere at the instant shown here. The first difference to note is that unlike the F5 V star, the photospheric temperature structure of the K5 V star is almost unaltered by the acoustic waves. This result can be found both by inspecting the time-dependent temperature structure and the velocity, which remains very small in the photosphere.

The reason for these differences are both the higher photospheric gas densities (by about a factor of 2) in the K5 V star and the smaller acoustic energy flux. In Table 1 we see that the initial acoustic energy flux of the K5 V star is about 1/57 of the much hotter F5 V star. As a consequence, the wave amplitude in the K5 V star is reduced to 0.08 times the value of the F5 V star model. Owing to this small wave amplitude, the photospheric temperature structure of the K5 V star is very close to radiative equilibrium. Therefore, no significant radiative damping occurs at photospheric levels for the waves (see Fig. 2). This is amplified by the much decreased radiative damping zone for this star, which only extends to $m_L \simeq 7.5$ g cm^{-2}. Noticeable radiative cooling rates are found only in postshock regions in the upper part of the atmosphere. Owing to the much smaller wave amplitudes, the point of shock formation is shifted to greater heights as it now occurs at $m = 0.01$ g cm^{-2}. The limiting strength of the shocks in the K5 V star is $\eta^{\rm lim} = 0.91$, which is larger than for the hotter star and

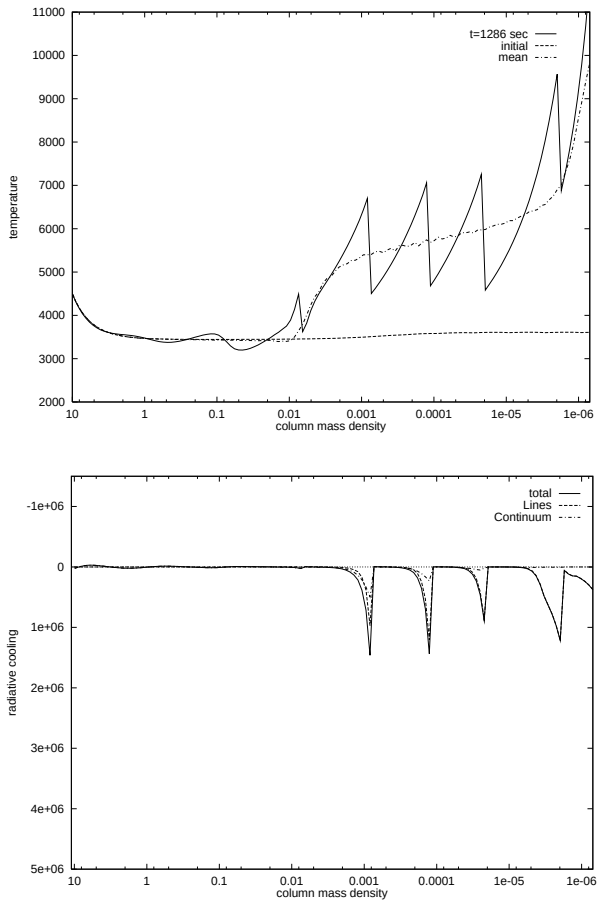

FIG. 2.—Same as Fig. 1, but now for the K5 V star after $t = 1286$ s

closer to the value given by equation (3). Whereas in the F5 V star the chromospheric temperature rise after shock formation leads to increased radiative damping, the temperature rise after shock formation is much more pronounced in the K5 V star. This is due to the fact that in the latter star, the position of shock formation is 2 orders of magnitude in units of mass column density above the radiative damping zone, while for the F5 V star it is at or below of this zone.

Note that the limiting shock strength behavior is not found at the early stage of the stellar wave computations, which is dominated by the atmospheric energy and momentum transfer of the first shock. As this shock enters a completely undisturbed medium, it triggers significant oscillations particularly at larger atmospheric heights. As these switch-on effects are physically unrealistic, they have been purposely ignored when time-averaged quantities are calculated and compared with observations.

3.2. *Chromospheric Line Emission*

The chromospheric line emission for the Mg II *k* and Ca II K line is calculated for each time step of the time-dependent wave calculation. To determine the energy losses caused by spectral line radiation, the emissions are calculated under the approximation of CRD. In this approximation, emission and absorption profiles are identical. On the other hand, the CRD approximation is insufficient to describe spectral line profiles (see, e.g., Ayres & Linsky 1976; Drake & Linsky 1983; Judge 1990). This approximation must therefore be avoided especially when theoretical line profiles are compared with observations. More realistic results are achieved when PRD is used. Here one allows for coherent scattering in the line wings, while in the line cores, complete redistribution dominates. In PRD, the emission and absorption profiles are no longer identical. This effect leads to a reduction of the line wings compared to CRD, where photons absorbed in the line core are permitted to leak out at the far line wings resulting in an enhanced energy loss.

For the solution of the time-dependent energy balance, the CRD approximation has been used for the calculation of the Mg II *k* radiation losses to simulate the *total* radiation losses in the middle and upper chromosphere. After the time-dependent wave computation has been completed, we subsequently compute lines and continua, which were previously not included in the models. The computation of the Mg II *k* and Ca II K line spectra for individual phases of the waves can then be accomplished by using a full PRD treatment. Examples of line fluxes from Ca II and Mg II are shown in Figures 3, 4, and 5. For the chromosphere model of the F5 V star, the emerging line profiles at $t = 994$ s for Mg II *k* and Ca II K are displayed both in CRD and PRD. We also indicate the corresponding profile for the radiative equilibrium atmosphere. To minimize the need for computer time, the calculations for the PRD profiles are carried out for the inner parts of the line only. This is possible because the contributions of the line wings are greatly reduced for PRD compared to CRD, as can be seen in Figure 3. Both the Mg II *k* and Ca II K lines show the characteristic appearance of chromospheric emission line cores, as expected. Comparisons of the CRD profiles of both lines with those resulting from the PRD calculations show that the emission cores in PRD are much narrower for both lines. The relatively broad emission cores found in CRD are a result of the above-mentioned possibility of the

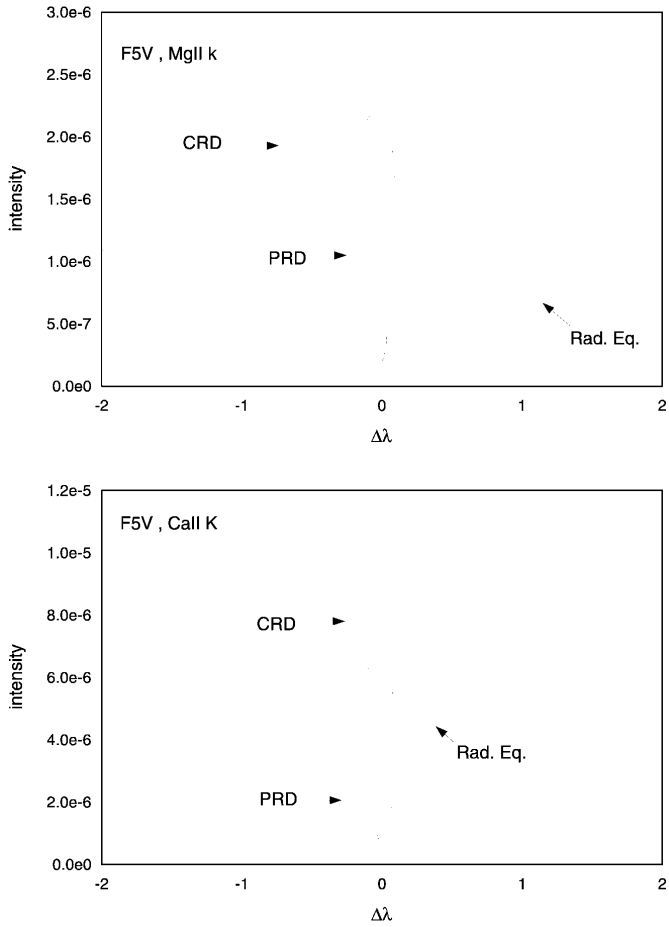

FIG. 3.—Mg II *k* and Ca II K line profiles (CRD and PRD) for the F5 V star after $t = 994$ s. The figures give intensity (ergs cm^{-2} s^{-1} sr^{-1} Hz^{-1}) vs. displacement $\Delta\lambda$ (Å) from the line center.

photons to escape through the line wings, thereby enhancing the wing intensities. In PRD, these photons are trapped in the line core and cannot escape because of the large optical depth. In addition, the frequency-dependent PRD source function in the core is modified relative to the frequency-independent CRD source function.

We now compare the results found for the F5 V chromosphere model with those for the K5 V model to discuss the systematic changes occurring at the main sequence. Figure 4 shows the emerging intensity profiles for the Mg II *k* and Ca II K lines for the K5 V star atmosphere model at $t = 590$ s. The first important difference is the wavelength scale of the two plots. The CRD as well as the PRD line profiles are much broader for the F5 V than for the K5 V star model. Owing to the different surface temperatures of these stars, the rest intensities visible in the line wings of the absorption profiles of the initial radiative equilibrium models are very different for both stars because of the temperature dependence of the Planck function. Furthermore, the differences in the radiative equilibrium profiles for the Mg II *k* and Ca II K in both stars are due to the frequency dependence of the Planck function. We note that the line profiles in CRD and PRD are not very different for the K5 V star, whereas the profiles for the F5 V star show much broader wings in CRD than in PRD. This difference is caused by the different number densities of Ca II and Mg II in the line formation regions of both stars. For the K5 V star, the number densities in the line formation region are relatively low, and

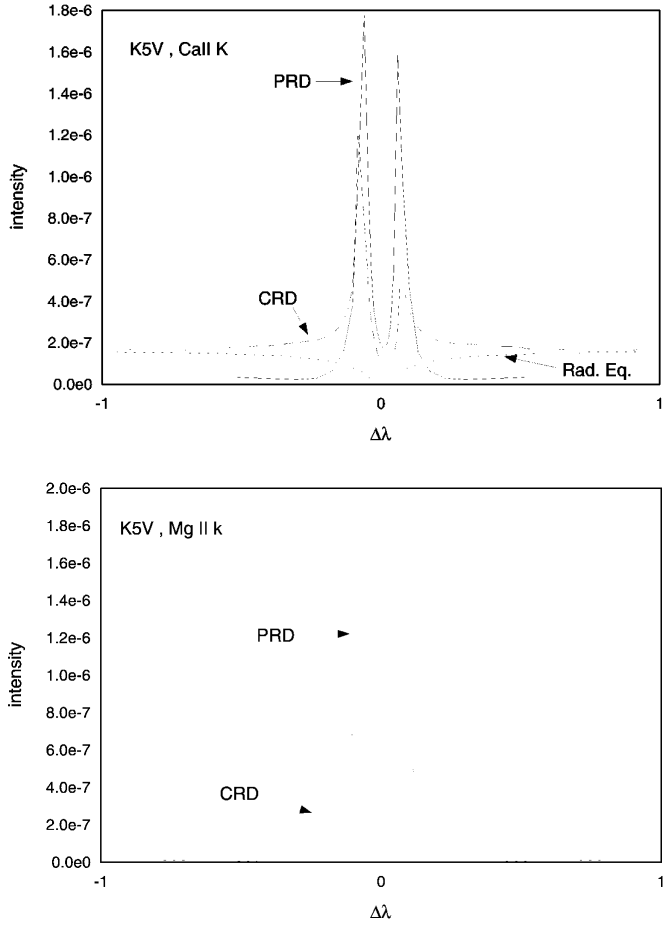

FIG. 4.—Same as Fig. 3, but now for the K5 V after $t = 590$ s

only the line cores are optically thick. The consideration of coherent scattering in PRD approximation affects only the line wings, and the differences between in CRD and PRD become thus relatively small for the K5 V star. This reflects the well-known result that CRD is a valid approximation for the Doppler core of the line.

The physical conditions in the line formation regions undergo large variations with time. The temperature and density changes occurring when a shock propagates through the emitting gas is accompanied by changes in magnitude and direction of the gas motions. This effect results in large time variations of the line profiles. An example of this behavior is given in Figure 5 for the Mg II k line for the F5 V star. It is found that the peak intensities vary by a factor of about 1.5 over the time span of one wave period, but the width of lines remains essentially constant. Note that all line profiles are computed without assuming additional line broadening by microturbulence. The line width of the Mg II k line of the F5 V star is $W_{\rm Mg} = 0.5$ Å and for the K5 V star is $W_{\rm Mg} = 0.2$ Å.

3.3. *Properties of Time-averaged Chromosphere Models*

In this section, we discuss the properties of time-averaged chromosphere models, which are determined by a dynamic equilibrium due to the balance of shock wave heating and radiative cooling. In typical cases, we have to wait until about 20–25 wave periods have propagated through the atmosphere that a dynamic equilibrium has been reached and the switch-on behavior caused by the start of the wave calculation has died out. At that point, the time-averaged quantities of the atmosphere do not change with time any longer. The physical variables at each height are then averaged over a time span of several wave periods. Figure 6 shows the run of the mean temperatures for our sample of stars. It displays the mean chromospheric temperatures as function of the mass column density m (g cm^{-2}) together with the radiative equilibrium temperatures of the initial atmosphere models. By comparing the mean chromospheric structures, one finds that all models show a temperature plateau with temperatures of about $T \simeq 5500$ K. This temperature is lowest for the F5 V star, where it is found to be only 5200 K. The highest temperature is reached in the model of the M0 V star with a mean temperature of 6000 K between $\log m = -3$ and $\log m = -5$ (cgs). The chromospheric temperature rise steepens with decreasing $T_{\rm eff}$ and is then shifted to smaller mass column densities.

This behavior is caused by the differences in the mechanical input fluxes, the wave amplitudes, and the different efficiency of radiative cooling, expressed also in the various extents of the radiation damping zones. The F5 V star with an input flux of $F_M = 6.56 \times 10^8$ ergs cm^{-2} s^{-1} has its point of shock formation at a much larger column mass density than the M0 V star, where shock formation is postponed owing to waves of much smaller amplitudes. Thus, the chromospheric temperature rise starts at larger mass column densities for main-sequence stars of higher effective

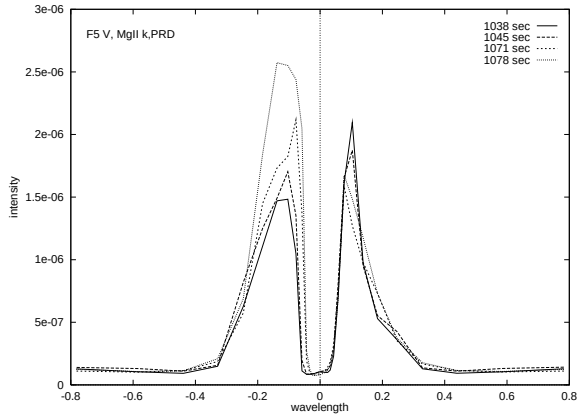

FIG. 5.—Intensity variations with time for the Mg II k line profile (PRD) for the F5 V star. The figures give intensity (ergs cm^{-2} s^{-1} sr^{-1} Hz^{-1}) vs. displacement $\Delta\lambda$ (Å) from the line center.

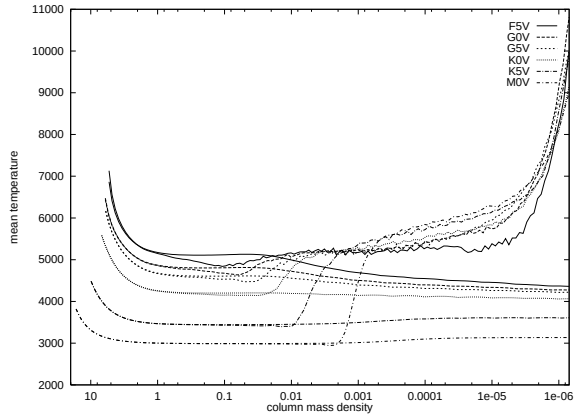

FIG. 6.—Time-averaged atmospheric temperature and initial radiative equilibrium temperature (K) vs. mass column density (g cm^{-2}) for the main-sequence stars calculated.

temperatures. As the shocks form in or close to the upper limit of the radiation damping zone, the F5 V star has larger radiative cooling losses by H^-, and the temperature increases more slowly than in the M0 V star. In this latter type of star, the sudden temperature increase by increased shock energy dissipation is not counterbalanced until line radiation starts to become effective.

The chromospheric temperature enhancement in the outer regions of the atmospheres is accompanied by a temperature depression near the point of shock formation and in the region underneath the temperature inversion. Shock heating strongly sets in only when the shock after its formation has grown to its full sawtooth shape. The mean temperature is depressed below the radiative equilibrium temperature despite the fact that the waves supply mechanical energy. This effect has been noted earlier (Ulmschneider et al. 1978; Kalkofen et al. 1984) and has been attributed to the nonlinearity of the Planck function with respect to the temperature. This depression is most easily understood if it is assumed that the opacity is constant. If one assumes further that the wave perturbs the temperature T about the steady state value $\bar{T}$ by the amount δT, i.e., $T = \bar{T} + \delta T$, the energy equation at the bottom of the chromosphere may be written as

$$T_0^4 = \bar{T}^4\left[1 + 4\overline{\left(\frac{\delta T}{\bar{T}}\right)} + 6\overline{\left(\frac{\delta T}{\bar{T}}\right)^2} + \cdots\right]. \qquad (5)$$

When the relative amplitude, $\delta T/T$, becomes sufficiently large, the nonlinear term forces the mean temperature T to be lower than the (initial) radiative equilibrium temperature T_0. Note, however, that in realistic cases the actual depression depends on the detailed temperature dependence of the opacity in the nongray non-LTE energy equation as well as the wave profile and the number of waves that have passed the temperature minimum region (if that no dynamic steady state has been achieved) (Kalkofen et al. 1984).

As the regions of large temperature depressions are also regions of intense radiative damping of the waves, it is not surprising that these large amounts of excess radiation supplied by the conversion of mechanical energy above the pure radiative equilibrium distribution have been accounted for in empirical chromosphere models as photospheric temperature enhancements in the temperature minimum regions (see, e.g., Ayres & Linsky 1975, 1976; Kelch et al. 1978; Kelch, Linsky, & Worden 1979; Kelch 1978; Linsky & Ayres 1978 among others; see also the review by Linsky 1980). It is precisely those earlier types of stars that show the largest photospheric temperature enhancements and also show the largest temperature depressions, which indicates that the temperature depressions in our models and the empirical photospheric temperature enhancements are two aspects of the same phenomenon.

The most extreme case of a temperature depression is found in the F0 V star. Having an effective temperature of $T_{\rm eff} = 7200$ K, this star is the hottest of our sample with an initial acoustic energy flux of $F_M = 1.2 \times 10^9$ ergs cm^{-2} s^{-1}. The temperature fluctuations are extremely large with values of $2\,\delta T \simeq 2000$ K. Owing to these fluctuations, the mean atmospheric temperature is depressed by 1000 K below the radiative equilibrium temperature (see Fig. 7). This temperature depression extents for more than two orders of magnitude in m. In the case of the F0 V star, it is found that almost the entire mean atmosphere has a temperature below the radiative equilibrium temperature. Only in the outermost parts of the model is a chromospheric temperature rise found. On the other hand, a semiempirical model that produces the same emission flux as the time-dependent model would definitely need a temperature inversion similar to those in the other models.

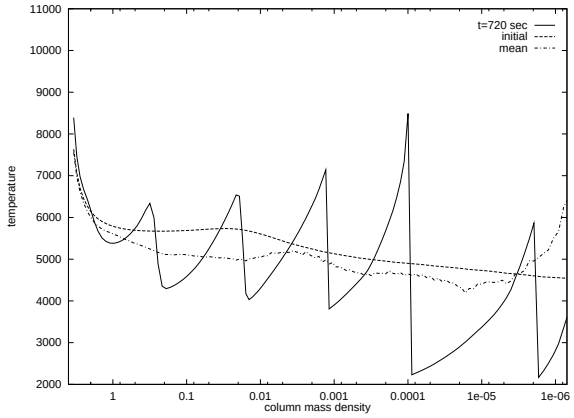

FIG. 7.—Snapshot showing the run of temperature (K) for the F0 V star as function of the mass column density (g cm^{-2}) after $t = 720$ s. The figure depicts the current temperature (*solid line*), the initial temperature (*dashed line*), and the mean (i.e., time-averaged) temperature (*dashed-dotted line*).

An important consequence of the nonlinearity of the chromospheric emission is that it is not possible to interpret the occurrence of chromospheric line emission simply as the result of an enhanced *mean* temperature in the line formation regions. These emission regions are found to be highly inhomogeneous and variable with time. Enhanced emission occurs when a shock propagates through the region of line emission. Therefore, the time-averaged emission is dominated by the short phases of greatly enhanced temperatures. This scenario was shown also to explain the chromospheric emission from the solar intranetwork regions (Carlsson & Stein 1995). In the view of these results, we can state that the "chromosphere" that is observed in the emission cores of the Mg II $h + k$ and Ca II H + K lines very likely consists of hot regions behind the shocks unrelated to a mean chromospheric temperature rise (if existent).

Once the chromosphere models have reached their final dynamical equilibrium state, the mean chromospheric heating rate is exactly balanced by mean radiative cooling. The resulting time-averaged cooling rate then reflects the height dependence of the time-averaged heating rate by the shocks. Figure 8 shows the time-averaged values of the cooling rates per gram (ergs s^{-1} g^{-1}) for the main-sequence stars. The extent of the radiative damping zones as well as the chromospheric heating rates are found to be systematically different for the different stars. This is due to the different temperature fluctuations and the resulting differences in the damping function D. The onset of the chromospheric temperature rises is found to be controlled by the cooling rates in the radiative damping zones of the stars. After the temperature plateaus are reached, the heating rates become constant with height. They are also found to be essentially the same for all stars, despite the largely different mechanical input fluxes F_M. Our models show a constant heating rate of $\simeq 3 \times 10^9$ ergs g^{-1} s^{-1}. This constant heating rate is consistent with results from the static semiempirical solar chromosphere model of Anderson & Athay (1989) who

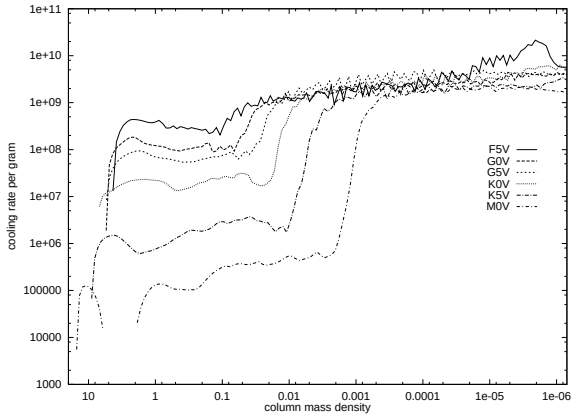

FIG. 8.—Time-averaged cooling rates per gram (ergs s^{-1} g^{-1}) vs. mass column density (g cm^{-2}) for the main-sequence stars calculated.

derived a value being a factor of 1.5 larger. The fact that the heating rate per gram remains constant follows directly from the assumption of shock heating by shocks of limiting strength.

Now let us compare the chromospheric energy flux emitted by Mg II $h+k$ and Ca II H + K with the initial acoustic energy flux input into the models. We find that the fraction of the acoustic input flux visible as chromospheric line emission increases with $B-V$. While a main-sequence star of spectral type F has a line emission flux $F_{\mathrm{Ca+Mg}}$ that is as small as $1/150 \times F_M^0$, a star of spectral type M has a Mg II plus Ca II emission flux of $1/20 \times F_M^0$ (see Fig. 9). Almost all of the rest of the flux goes into H^- continuum emission. The amount of flux leaving the computational domain is usually much less than 0.1% of the wave energy flux entering the atmosphere. This result demonstrates that the efficiency of acoustic heating increases with increasing $B-V$, which is also consistent with more recent results of acoustic energy generation by Ulmschneider et al. (1996).

3.4. *Test of the Ayres Scaling Law*

One way of assessing the physical relevance of the mean thermal structure of the theoretical chromosphere models is to make a comparison with predictions of the T. R. Ayres scaling law. Ayres (1979) estimated the thickness and mean electron density of stellar chromospheres assuming time-independent structures chosen to explain the observed radiative emission losses. While taking an estimate for the base heating rate, Ayres was able to deduce the value for the mass column density at the temperature minimum region m_{TM}, which is determined by H^- cooling. He found that m_{TM} is related to the stellar parameters g and T_{eff} by

$$m_{\mathrm{TM}} \sim A \quad \text{with } A = \mathscr{F}^{-1/2}\left(\frac{g}{g_\odot}\right)^{-(1/2)}\left(\frac{T_{\mathrm{eff}}}{T_{\mathrm{eff},\odot}}\right)^{(7/2)\pm 1}, \quad (6)$$

where $g_\odot$ and $T_{\mathrm{eff},\odot}$ denote g and T_{eff} for the Sun and $\mathscr{F}$ is the activity parameter, which is $\simeq 1$ for the least active stars (notably chromospheric basal flux stars) and $\simeq 10$ for stars with very active chromospheres.

This scaling law has been successfully tested in comparison with semiempirical chromosphere models that assume smooth functions for the atmospheric temperature, density and velocity. These semiempirical models make no assumptions regarding the chromospheric heating mechanism. The ± 1 uncertainty in the T_{eff} exponent was included to consider the spread of observed Mg II emission losses if measured in units of the stellar bolometric luminosity. In fact, if found that the mean thermal structure of our time-dependent chromosphere models is consistent with the Ayres scaling law, it would provide an important *independent* test about the reliability of the heating models calculated.

Figure 10 shows the behavior of m_{TM} as function of the scaling parameter A with $\mathscr{F} = 1$. We find that the mass column densities at the temperature minimum of our models obey an almost perfect linear fit consistent with equation (6). In that respect we were even able to disregard the ± 1 uncertainty in the T_{eff} exponent proposed by Ayres. Note that we considered only the models for the main-sequence stars between spectral type F5 V and M0 V without including the F0 V star. This star does not show a significant chromospheric temperature increase (see Fig. 7), and no pronounced temperature minimum could be identified. The slope of the linear fit in Figure 10 is 0.053 g cm^{-2} in close agreement with the semiempirical result for Procyon (F5 IV–V), which is 0.046 g cm^{-2} (Ayres, Linsky, & Shine 1974). Note that most other stars studied by J. L. Linsky and his group at that particular time have a much

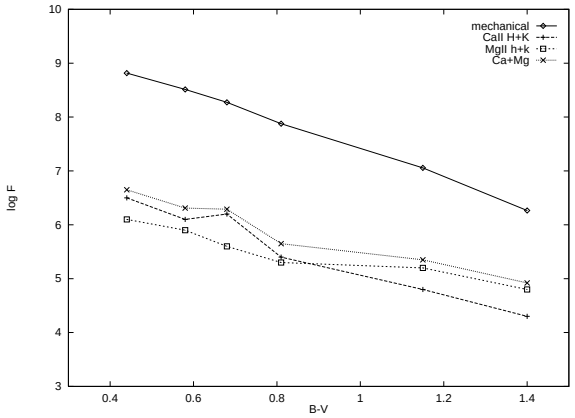

FIG. 9.—Comparison of the chromospheric emission fluxes of the main-sequence stars with the acoustic input fluxes. The chromospheric emission fluxes are given by the theoretical models.

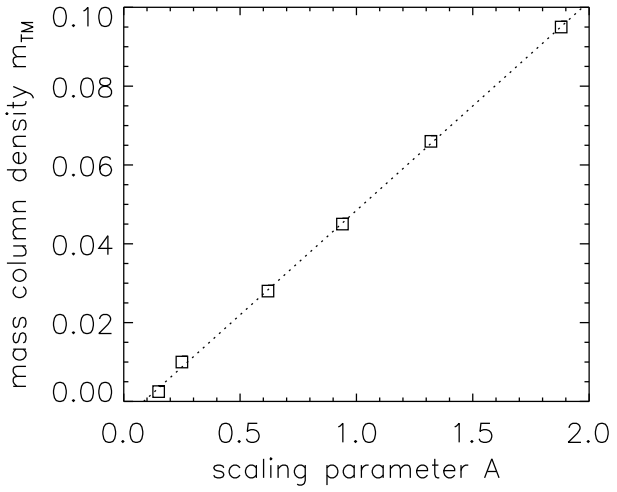

FIG. 10.—Mass column density (g cm^{-2}) at the theoretical temperature minima of the main-sequence stars indicated by boxes vs. scaling parameter A given by Ayres (1979). Also shown is a linear fit to the data.

higher chromospheric activity level and can thus not be used for comparison.

3.5. *Results for Late-Type Giants*

We now examine the dependence of chromospheric properties including the generation of chromospheric emission fluxes on the stellar surface gravity g. We calculated models for two giants, a K0 III giant with $T_{\rm eff} = 4750$ K and $\log g = 2.13$ (cgs) and a K5 III giant with $T_{\rm eff} = 3950$ K and $\log g = 1.74$ (cgs) (see Table 1). We again use the acoustic energy fluxes and the wave periods of Bohn (1981, 1984). Figure 11 shows a snapshot of the time-dependent wave calculation together with the mean and initial (i.e., radiative equilibrium) temperature distribution for the K5 III star. Most of the shocks in these models are quite small. The larger shocks are a direct consequence of shock merging, which is found even in the cases of monochromatic wave models when small wave periods are considered (Cuntz 1988; Rammacher & Ulmschneider 1992). Note that the photospheric mass column densities in giants are much larger than in main-sequence stars owing to their larger atmospheric extents as a consequence of the lower surface gravities and the pressure dependence of the opacity.

Further properties of the giant star chromospheres include the much higher radiation damping efficiency of the atmospheres and the larger extent the radiative damping zones (Ulmschneider 1988). The radiation damping zone of the K0 III giant extends up to $m_L \simeq 1.8$ g cm^{-2} and in the K5 III giant (Fig. 11) up to 0.5 g cm^{-2}. In comparison, that zone extends only up to $m_L \simeq 7.5$ g cm^{-2} in the K5 V star (Fig. 2). This strong radiation damping in giant stars restricts the ability of the acoustic waves to carry energy to the higher atmospheric layers. In addition, it ensures that the large gravity dependence of the acoustic flux generation in subphotospheric layers does not translate into a similar extensive gravity dependence of the chromospheric line emission, which has been confirmed by calculating time-dependent acoustic heating models (Ulmschneider 1989).

Figure 12 shows the emergent line profile of the Mg II k line for the K5 III chromosphere model. Owing to the large shocks formed by overtaking, the variability of the line profile is larger than for the main-sequence stars. Yet when the mean chromospheric emission fluxes for Ca II H + K and Mg II $h + k$ are computed, the emission fluxes are very similar to those of the K5 V star and are consistent with the basal flux limits (see § 4). Our time-dependent models thus reproduce the observational fact that dwarf and giant stars show essentially the same basal emission flux independent of gravity (Schrijver 1987; Rutten et al. 1991).

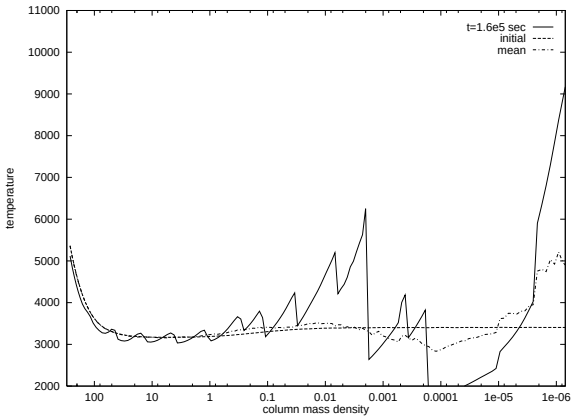

FIG. 11.—Snapshot showing the run of temperature (K) for the K5 III star as function of the mass column density (g cm^{-2}) after $t = 1.6 \times 10^5$ s. The figure depicts the current temperature (*solid line*), the initial temperature (*dashed line*), and the mean (i.e., time-averaged) temperature (*dashed-dotted line*).

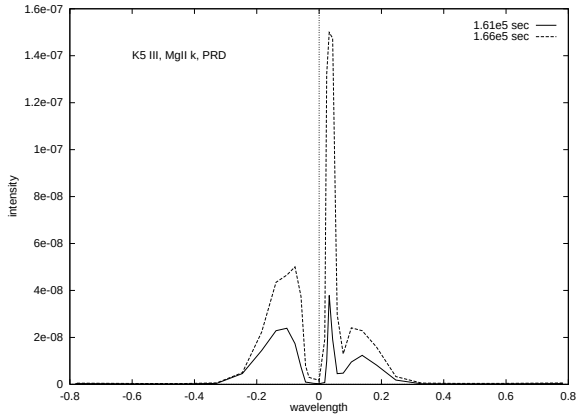

FIG. 12.—Mg II k line profiles (PRD) for the K5 III star after $t = 1.61 \times 10^5$ and 1.66×10^5 s. The figure gives intensity (ergs cm^{-2} s^{-1} sr^{-1} Hz^{-1}) vs. displacement $\Delta\lambda$ (Å) from the line center.

In the limit of weak shocks, the mechanical energy flux of a shock wave can be written as (Ulmschneider 1970)

$$F_M \simeq \tfrac{1}{12}\gamma p_0 c_s \eta^2 , \tag{7}$$

where p_0 is the undisturbed pressure, c_s is the sound speed, and η is the shock strength parameter. The change of mechanical energy flux with height is thus given as

$$\frac{dF_M}{dz} = \frac{1}{12}\frac{(\gamma+1)\gamma}{P} p_0 \eta^3 = -\frac{F_M}{L_A} , \tag{8}$$

where L_A denotes the acoustic damping length given by

$$L_A = \left[\frac{\gamma p_0 c_s^2}{12(\gamma+1)^2}\right]^{1/2} F_M^{-1/2} P = \frac{c_s P}{(\gamma+1)\eta} . \tag{9}$$

Here P is the wave period as usual. In case the shock waves have achieved their limiting strength $\eta^{\rm lim}$, the shock heating rate per gram can then be computed by

$$\frac{1}{\rho}\frac{dF_M}{dz} \simeq \frac{4\pi^2}{75}\frac{\gamma}{(\gamma+1)^2} c_s g . \tag{10}$$

Here we have assumed again that the shock strengths do not deviate substantially from the values given by the weak shock limit (see eq. [3]), which is strictly valid only in case of idealized atmospheres and of shocks with relatively small strength (see § 3.1). We also made use of the assumption that the wave period in our models is $P = 0.2 P_A$ (see § 2).

From equation (10), we expect a significant dependence of the limiting shock strength heating rate on gravity if the heating rate is normalized to the density. For the K0 III star, the theoretical heating rate according to equation (10) is 1.5×10^7 ergs g^{-1} s^{-1}, which is a factor of $\simeq 200$ lower than in main-sequence stars. For the K5 III star, the reduction factor is $\simeq 540$. Despite the fact that our models are not completely in dynamical equilibrium, we find that the time-averaged cooling rates (per gram) shown in Figure 13 roughly agree with the theoretical estimates of the heating rates of equation (10) (see comparison of Figs. 8 and

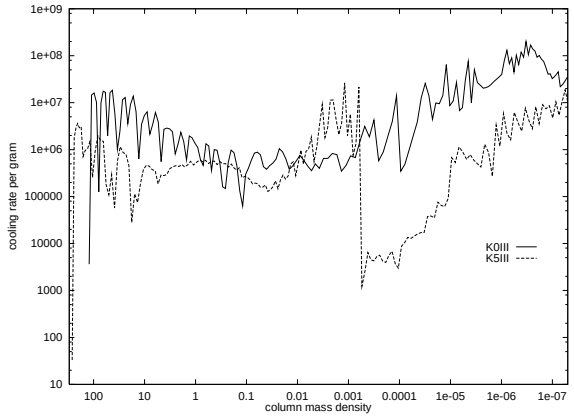

FIG. 13.—Time-averaged cooling rates per gram (ergs s^{-1} g^{-1}) vs. mass column density (g cm^{-2}) for the K0 III and K5 III giant star.

13). Owing to the strong radiative damping in the giant stars, however, the time-averaged chromosphere models do not show a significant temperature rise over a large portion of the atmosphere. The shocks cannot heat up the atmosphere, and the temperatures thus stay near the equilibrium values. A similar result for a giant with $T_{\rm eff} = 5012$ K and $\log g = 3$ has been found by Cuntz et al. (1994). In that paper, the authors presented time-dependent chromosphere models with different metallicities. They found that their model with solar abundances did also not exhibit a chromospheric temperature rise over a considerable distance.

4. COMPARISON WITH OBSERVATIONS

We now discuss how our theoretical results compare with observations. Schrijver (1987), Schrijver et al. (1989), and Rutten et al. (1991), among others, presented a detailed statistical analysis of flux-flux and flux-color relations derived from selected emission lines for a large sample of late-type stars. They argued that these relations can best be understood when assumed that the stellar emission line fluxes consist of a *basal* component, which is independent of magnetic activity, and a *magnetic* component depending on rotation and thus on the age of the star. They identified the lower limits in the chromospheric emissions of Ca II H + K and Mg II $h + k$ as well as several other lines as an intrinsic property of the stars, which is likely be attributable to acoustic shock wave heating.

These findings are sufficient ground to confront our theoretical results with observations. As the results of Schrijver and Rutten et al. do not give any information about the time resolution of the heating process, we calculate the time-averaged emission flux of each line. From each stellar model, we thus compute the emergent line profiles of Mg II k and Ca II K for a large number of time steps both in CRD and PRD. As shown in Figure 5, the emerging line profiles vary with time according to the phase of the wave. We therefore integrate the emission cores over wavelength between the k_1 and K_1 minima, respectively, to obtained the total emergent intensities $I^+_{\rm Mg}$ and $I^+_{\rm Ca}$. In the two-beam approximation, the total emission flux is then given by $F = 2\pi\mu I^+$ with the angle cosine $\mu = 1/3^{1/2}$. We now average each flux over time to obtain the mean chromospheric emission in Ca II K and Mg II k.

The fluxes for Ca II and Mg II given by Schrijver and Rutten et al. are essentially Ca II H + K and Mg II $h + k$ fluxes. Therefore, when calculating the total Mg II and Ca II fluxes, we also have to consider the contribution of the Mg II h and Ca II H lines. In the optically thin case, we would have to multiply the flux of Mg II k by a factor of 1.5, because $F_k : F_h = 2:1$. As we do not have the optically thin case, this would produce unrealistic results. Stencel et al. (1980) measured Mg II h and k flux ratios for a sample of 54 cool stars. On average, they found $F_k : F_h = 1.3:1$, which would correspond to a conversion factor of 1.8. Regarding the conversion factor of Ca II, the situation is even more complex as the observed Ca II fluxes are usually strongly contaminated by contributions from the photospheric radiation fields, which differ largely with the spectral type and luminosity class of the star (see, e.g., Schrijver et al. 1989; Duncan et al. 1991). Furthermore, the calibration of the continuum flux at the position of the Ca II H and K lines is often relatively uncertain, particularly in cases in which detailed model atmospheres do not exist. Owing to the lack of multilevel simulations for the Mg II and Ca II line fluxes, it is therefore most straightforward to use a conversion factor of 2 in this case. Note that the data for Ca II of Rutten et al. (1991) have been corrected for the photospheric contributions. To account for this effect, we adopt a similar correction by subtracting the equilibrium flux F_0 from the time-averaged total emission flux. For Mg II, no such correction needs to be applied as the photospheric contributions are negligible.

We now compare the theoretical emission fluxes for Mg II and Ca II with the results of Rutten et al. In Figure 14 we plot the averaged total Mg II and Ca II emission fluxes into Figures 1*b* and 1*a* of Rutten et al. It is seen that our PRD fluxes satisfy reasonably well the observed common basal flux limit for the different types of main-sequence stars and also for the giants. The CRD line fluxes are not realistic in this case, as expected. We only give these fluxes for tutorial reasons. Note however, both from Figure 14 and Figures 3 and 4, that the contribution to the emission of the CRD flux is much closer to the PRD flux for the Ca II than for the Mg II lines. The differences between the PRD Mg II and Ca II line fluxes and the respective basal flux limits are between 0.1 and 0.5 in the logarithm. This is quite astonishing as we are dealing with completely different types of stars, which have vastly different atmospheric structures leading to different hydrodynamic phenomena regarding the propagation of the acoustic waves. It is possible that the remaining disagreements between the theoretical basal flux line and our theoretical results are in part also caused by technical oversimplifications in our hydrodynamic models and the treatment of radiation. In case of the Ca II lines, the influence of multilevel radiative transfer effects on the line formation is also well established.

Figure 15 compares the theoretical Mg II emission with results from other theoretical and observational studies. In addition to the basal flux line of Rutten et al. (1991), we also display an earlier version of the line given by Schrijver (1987). The upper limits of the fluxes given for very cool dwarfs as obtained by Byrne (1993) and Doyle et al. (1994) are also displayed. Byrne presented estimates of the Mg II losses from the dM(e) star Gl 105B. This star at $B-V = 1.59$ has a Mg II $h + k$ emission of 8×10^3 ergs cm^{-2} s^{-1}, which lies within the range permitted by the data of Rutten et al., although it clearly puts a significant constraint on the basal flux value. The subsequent study of Doyle et al. for four extremely inactive M dwarfs yielded

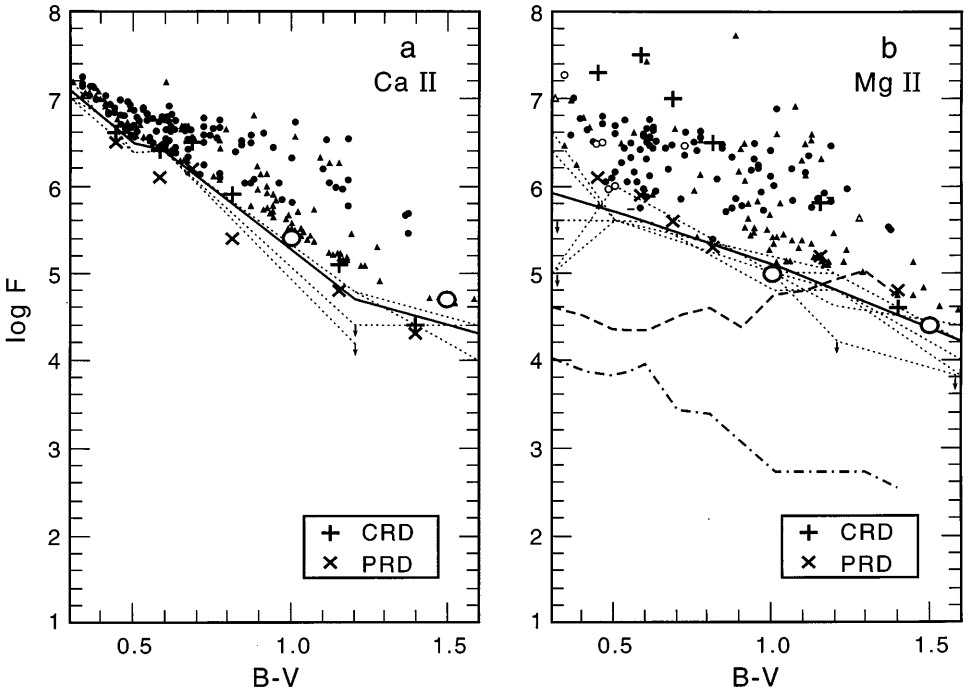

FIG. 14.—Theoretical emission fluxes of Mg II $h + k$ and Ca II H + K compared with empirical fluxes given by Rutten et al. (1991). Our results for the main-sequence stars are shown as plus signs (CRD) and crosses (PRD). The PRD emission fluxes of the two giant stars are given as circles.

even lower Mg II surface fluxes. They found that Gl 813 has a Mg II $h + k$ of less than 4×10^3 ergs cm^{-2} s^{-1}, which reduces the basal emission flux for this type of star by a factor of 2 (Schrijver 1995). Figure 15 also gives the results for the basal flux limits for inactive noncoronal giant stars obtained by Judge & Stencel (1991). This line turns out to be a perfect match for the theoretical result of the K5 III star, whereas the Mg II emission of the K0 III star is found to be consistent with the Rutten et al. limit, which is also valid for giants. The fact that the theoretical Mg II emission fluxes are essentially the same for dwarfs and giants despite the fact that giants have an increased initial acoustic energy flux can be explained by the increased efficiency of radiative damping in giant stars, particularly in the H^- continuum. This effect leads to similar amount of wave energy present in the Mg II line formation region in both types of stars (Ulmschneider 1988, 1989; Cuntz et al. 1994).

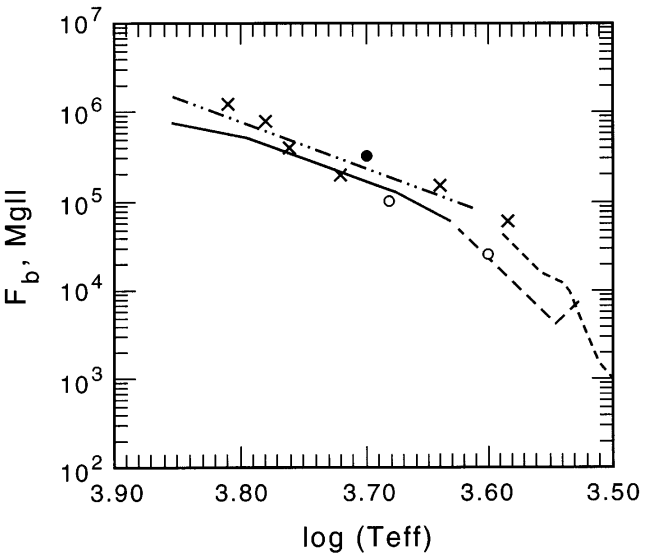

FIG. 15.—Diagram showing the basal flux limit for Mg II $h + k$ as function of stellar effective temperature together with results from observations. The solid line shows the results from Rutten et al. (1991), whereas the double-dotted/dashed line indicates earlier results from Schrijver (1987). The long-dashed line represents the upper limits derived for very cool dwarfs given by Doyle et al. (1994). The short-dashed line shows the Mg II basal flux limit for giants from the sample of Judge & Stencel (1991). The crosses and open circles represent theoretical results from this work for main-sequence stars and giants, respectively. The closed circle at log $T_{\rm eff} = 3.70$ shows the theoretical result of Cuntz et al. (1994) ignoring the very small differences in the Mg II flux due to the different atmospheric metallicities considered (modified version of Fig. 5 of Schrijver 1995).

The close agreement of our theoretical results with the observed basal flux limits, extending over nearly 2 orders of magnitude in emission flux, is indeed significant evidence that acoustic waves are most likely responsible for the main energy input in the chromospheres of inactive main-sequence stars and giants. Despite the obvious limitations of our calculations, which include (1) the usage of monochromatic waves instead of acoustic frequency spectra, (2) the approximation of the time-dependent middle chromospheric radiative cooling function by a single line Mg II k in CRD, and (3) the neglect of the detailed treatment of the hydrogen ionization balance including noninstantaneous effects (see, e.g., Carlsson & Stein 1992, 1995), we strongly feel that the above-mentioned agreement is very satisfactory.

5. CONCLUSIONS

We computed time-dependent models of chromospheres for main-sequence stars between spectral type F0 V and M0 V and for two giant stars. Starting from initial atmosphere models in radiative equilibrium, we introduced monochromatic acoustic waves, which were followed to the point of

shock formation and beyond. The wave computations included radiative damping to attain time-averaged steady state solutions of the wave-supported atmospheres. These atmospheres were studied in detail and compared with results from semiempirical modeling. By analyzing the time-dependent wave models, we also calculated time-averaged line fluxes for Mg II *k* and Ca II K assuming CRD and PRD. The PRD line fluxes were then compared with observations. Our principal results can be summarized as follows:

1. Owing to the propagation and dissipation of acoustic wave energy, chromospheric temperatures are found in all stars calculated. The chromospheric temperature structures occur both as apparent and as true mean temperature enhancements, depending on the type of the star.

2. The true mean temperature enhancements are the result of the balance of shock heating and radiative cooling with no significant wind flows generated. In stars of earlier spectral types (such as the F0 V star), the mean chromospheric temperature enhancement was found to be relatively small or nonexisting, as shock formation occurs within or close to the radiative damping zones. On the other hand, in stars of later spectral types (such as the M0 V star), relatively large chromospheric temperature enhancements were found.

3. The large core emission in the Ca II and Mg II lines produced by the postshock temperature spikes simulates an apparent chromospheric temperature rise, which is found to be particularly large in early late-type main-sequence stars. This core emission flux has previously been used to construct time-independent semiempirical chromosphere models, which assume a smooth behavior of atmospheric temperature, density, and velocity as function of height.

4. In earlier types of stars, we found regions of large temperature depressions near the point of shock formation, which are also regions of intense radiative damping of the waves. In empirical chromosphere models, these large amounts of excess radiation have been identified as temperature enhancements in the temperature minimum regions (Linsky 1980; and references therein). Our models indicate that the temperature depressions and the empirical temperature enhancements are two aspects of the same phenomenon, which is most extreme in the F0 V star.

5. The radiative emission is found to be strongly peaked behind the shocks largely unrelated to the structure of the mean (i.e., time-averaged) atmosphere, which is consistent with earlier findings (see, e.g., Cuntz & Judge 1990). This scenario has been shown also to explain the chromospheric emission from the solar intranetwork regions by Carlsson & Stein (1995). Clearly, chromospheric emission does not require a *classical* chromosphere with a mean temperature rise—a result of particular relevance for the formation and interpretation of chromospheric emission lines.

6. We found that the efficiency of acoustic energy transfer from the photosphere to the chromosphere increases with decreasing $T_{\rm eff}$ for the main-sequence stars. This is due to the extent of the radiative damping zones, in which the waves lose their energy via radiative damping. This effect is particularly relevant in stars of spectral type K0 V and earlier. For main-sequence stars of later spectral types, the wave energy flux remains almost unaltered by photospheric radiative damping.

7. Radiative damping is even more significant for giant stars. It is found that the K0 III and K5 III stars have essentially the same chromospheric emission as the main-sequence stars of similar spectral type, despite the fact that the initial acoustic energy fluxes are larger by a factor of 5.3 and 8.8, respectively. This result is in agreement with findings of Ulmschneider (1988, 1989), which show that waves in late-type giants suffer far more energy loss by radiative damping than main-sequence stars of similar effective temperature.

8. The position of the temperature minima found in time-averaged chromosphere models of stars between spectral type F5 V and M0 V obey the simple linear scaling law of Ayres (1979) deduced for semiempirical chromosphere models of stars with a minimum level of chromospheric activity. These empirical models have been computed on the basis of observational data and are therefore independent of any assumptions regarding the chromospheric heating mechanism. For the stellar model of spectral type F0 V, no significant temperature enhancement was found, and thus no pronounced temperature minimum has been identified.

9. As we have adopted monochromatic shock waves, we found that the shock strengths as well as the density, pressure, velocity, and temperature jumps across the shocks essentially follow the simple analytical expressions for all stars, which are solely determined by the ratio of the wave period to the acoustic cutoff period (Brinkley & Kirkwood 1947; Ulmschneider 1970). These quantities are found to be largely identical in all stars calculated. The height dependence of the chromospheric heating rates is found to obey the limiting shock strength behavior of the waves.

10. The height-dependent heating rates are found to be consistent with the results from the static semiempirical solar chromosphere model of Anderson & Athay (1989) considering the technical differences between both types of models. For the two giant stars, the atmospheric heating rates are lower by a factor of 200 and 540, respectively, consistent with the prediction by the limiting shock strength property.

11. Because of the limiting shock properties of the computed monochromatic acoustic waves, we do not expect that our results will change much when updated results for the initial acoustic energy fluxes (Ulmschneider et al. 1996) are considered. This situation may change however, as soon as acoustic frequency spectra are considered, which is our field of future research. Earlier results showing the impact of frequency spectra on the dynamic structure of stellar chromospheres are given by Fleck & Schmitz (1993), Kalkofen et al. (1994), Sutmann & Ulmschneider (1995a, 1995b), and Theurer, Ulmschneider, & Cuntz (1997).

12. It has been the main purpose of this work, to compare the theoretical emission fluxes for Mg II and Ca II with observations. In particular, we attempted to fit the basal flux line original proposed by Schrijver (1987) and Rutten et al. (1991). We found that our PRD Mg II and Ca II line fluxes fit the Mg II and Ca II basal flux lines over nearly 2 orders of magnitude within about a factor of 2 both for the main-sequence stars and giants. This result is particularly remarkable as the stars calculated vastly differ in their atmospheric structures and the radiation-hydrodynamic properties of the waves.

The good agreement between the theoretical and empirical emission fluxes is strong evidence for the view that the main portion of the chromospheric energy input in chromo-

spheric basal flux stars is due to acoustic waves. This result is also consistent with the efficient generation of acoustic energy by stellar convection. Further evidence in favor of acoustic heating has been provided by a very recent paper of Peterson & Schrijver (1997). They analyzed Mg II spectra of nine very old metal-poor solar-type stars, whose great age and slow rotation clearly argue against significant magnetic heating. They found (1) that all stars exhibit a level of Mg II emission commensurate with the Mg II basal flux limit and (2) that despite interstellar absorption seven stars had asymmetric Mg II emission peaks with the blue peak stronger than the red. This latter behavior is clearly expected from acoustic heating models owing to the correlation among density, temperature, and velocity.

On the other hand, other evidence also exists that shows that most stars should also possess magnetic surface structure. In case of main-sequence stars, the presence of magnetic field coverage can be derived from the rotation chromospheric-activity relation (see, e.g., Rutten 1986) or simply from the presence of stellar coronae, which definitely cannot be heated acoustically (Vaiana et al. 1981; Stępień & Ulmschneider 1989; Hammer & Ulmschneider 1991; see also recently Schmitt 1997). In case of late-type giants, stellar magnetic fields might also be present, as acoustic waves are found to be incapable of explaining the magnitude of chromospheric turbulence (Judge & Cuntz 1993; Harper, Bennett, & Cuntz 1998) as deduced from *HST*-GHRS data (Carpenter et al. 1991) and might also fail to produce reasonable mass loss rates (Hartmann & MacGregor 1980; Cuntz 1990; Sutmann & Cuntz 1995); here Alfvén wave–driven winds may operate (see, e.g., Rosner et al. 1995). The reconciliation of this magnetic picture with the now relatively well founded acoustic heating picture in explaining the chromospheric basal flux limits is very much to be desired.

The authors are thankful to M. Carlsson for helpful comments. This work has been supported by the German Research Foundation (DFG) through project Ul 57/14-1 (B. B., P. U.), through a stipend provided by the state of Baden-Württemberg (B. B.), and by the NASA Astrophysical Theory Program NAG 5-3027 to the University of Alabama in Huntsville (P. U., M. C.). Further support was provided by NASA through grant AR-5285.02-93A from the Space Telescope Science Institute, which is operated by the Association of Universities for Research in Astronomy, Inc., under NASA contract NAS 5-26555 (M. C.).

REFERENCES

Anderson, L. S., & Athay, R. G. 1989, ApJ, 336, 1089
Ayres, T. R. 1979, ApJ, 228, 509
Ayres, T. R., & Linsky, J. L. 1975, ApJ, 200, 660
———. 1976, ApJ, 205, 874
Ayres, T. R., Linsky, J. L., & Shine R. A. 1974, ApJ, 192, 93
Bohn, H. U. 1981, Ph.D. thesis, Univ. Würzburg
———. 1984, A&A, 136, 338
Brinkley, S. R., & Kirkwood, J. G. 1947, Phys. Rev., 71, 606
Buchholz, B., Hauschildt, P., Rammacher, W., & Ulmschneider, P. 1994, A&A, 285, 987
Byrne, P. B. 1993, A&A, 278, 520
Carlsson, M., & Stein, R. F. 1992, ApJ, 397, L59
———. 1995, ApJ, 440, L29
Carpenter, K. G., Robinson, R. D., Wahlgren, G. M., Ake, T. B., Ebbets, D. C., Linsky, J. L., Brown, A., & Walter, F. M. 1991, ApJ, 377, L45
Charbonneau, P., Schrijver, C. J., & MacGregor, K. B. 1997, in Cosmic Winds and the Heliosphere, ed. J. R. Jokipii et al. (Tucson: Univ. of Arizona Press), 677
Cuntz, M. 1988, Ph. D. thesis, Univ. Heidelberg
———. 1990, ApJ, 353, 255
———. 1996, in IAU Symp. 176, Stellar Surface Structure, ed. K. G. Strassmeier & J. L. Linsky (Dordrecht: Kluwer), 393
Cuntz, M., Deeney, B. D., Brown, A., & Stencel, R. E. 1996, ApJ, 464, 426
Cuntz, M., & Höflich, P. 1998, in preparation
Cuntz, M., & Judge, P. G. 1990, in ASP Conf. Proc. 9, Cool Stars, Stellar Systems and the Sun, Proc. Sixth Cambridge Workshop, ed. G. Wallerstein (San Francisco: ASP), 61
Cuntz, M., Rammacher, W., & Ulmschneider, P. 1994, ApJ, 432, 690
Cuntz, M., & Ulmschneider, P. 1988, A&A, 193, 119
Doyle, J. G., Houdebine, E. R., Mathioudakis, M., & Panagi, P. M. 1994, A&A, 285, 233
Drake, S. A., & Linsky, J. L. 1983, ApJ, 273, 299
Duncan, D. K., et al. 1991, ApJS, 76, 383
Dupree, A. K., Hartmann, L., & Smith, G. H. 1990, ApJ, 353, 623
Fleck, B., & Schmitz, F. 1993, A&A, 273, 671
Gouttebroze, P. 1986, A&A, 160, 195
Gray, D. F. 1991, in Angular Momentum Evolution of Young Stars, ed. S. Catalano & J. R. Stauffer (Dordrecht: Kluwer), 183
Hammer, R., & Ulmschneider, P. 1991, in Mechanisms of Chromospheric and Coronal Heating, ed. P. Ulmschneider et al. (Berlin: Springer), 344
Harper, G. M., Bennett, P. D., & Cuntz, M. 1998, ApJ, submitted
Hartmann, L., & MacGregor, K. B. 1980, ApJ, 242, 260
Hünerth, G., & Ulmschneider, P. 1995, A&A, 293, 166
Judge, P. G. 1990, ApJ, 348, 279
Judge, P. G., & Cuntz, M. 1993, ApJ, 409, 776
Judge, P. G., & Stencel, R. E. 1991, ApJ, 371, 357
Kalkofen, W., Rossi, P., Bodo, G., & Massaglia, S. 1994, A&A, 284, 976
Kalkofen, W., Ulmschneider, P., & Schmitz, F. 1984, ApJ, 287, 952
Kelch, W. L. 1978, ApJ, 222, 931
Kelch, W. L., Linsky, J. L., Basri, G. S., Chiu, H.-Y., Chang, S.-H., Maran, S. P., & Furenlid, I. 1978, ApJ, 220, 962
Kelch, W. L., Linsky, J. L., & Worden, S. P. 1979, ApJ, 229, 700
Kneer, F. 1980, A&A, 87, 229
Kumar, P. 1994, ApJ, 428, 827
Landau, L. D., & Lifshitz, E. M. 1975, Fluid Mechanics (London: Pergamon)
Linsky, J. L. 1980, ARA&A, 18, 439
———. 1991, in IAU Colloq. 130, Lecture Notes in Physics 380, The Sun and Cool Stars: Activity, Magnetism, Dynamos, ed. I. Tuominen et al. (Berlin: Springer), 452
Linsky, J. L., & Ayres, T. R. 1978, ApJ, 220, 619
Mathioudakis, M., & Doyle, J. G. 1992, A&A, 262, 523
Middelkoop, F. 1982, A&A, 113, 1
Musielak, Z. E., Rosner, R., Stein, R. F., & Ulmschneider, P. 1994, ApJ, 423, 474
Narain, U., & Ulmschneider, P. 1990, Space Sci. Rev., 54, 377
———. 1996, Space Sci. Rev., 75, 453
Nordlund, Å., & Dravins, D. 1990, A&A, 228, 155
Pallavicini, R. 1992, in The Sun: A Laboratory for Astrophysics, ed. J. T. Schmelz & J. C. Brown (Dordrecht: Kluwer), 313
Pasquini, L., Pallavicini, R., & Pakull, M. 1988, A&A, 191, 253
Peterson, R. C., & Schrijver, C. J. 1997, ApJ, 480, L47
Rammacher, W., & Ulmschneider, P. 1992, A&A, 253, 586
Rosner, R., Musielak, Z. E., Cattaneo, F., Moore, R. L., & Suess, S. T. 1995, ApJ, 442, L25
Rutten, R. G. M. 1986, A&A, 159, 291
———. 1987, A&A, 177, 131
Rutten, R. G. M., Schrijver, C. J., Lemmens, A. F. P., & Zwaan, C. 1991, A&A, 252, 203
Schmitt, J. H. M. M. 1997, A&A, 318, 215
Schmitz, F. 1990, A&A, 229, 177
Schmitz, F., Ulmschneider, P., & Kalkofen, W. 1985, A&A, 148, 217
Schrijver, C. J. 1987, A&A, 172, 111
———. 1993, in ASP Conf. Proc. 40, Inside the Stars, ed. W. W. Weiss & A. Baglin (San Francisco: ASP), 328
———. 1995, A&ARev., 6, 181
Schrijver, C. J., Dobson, A. K., & Radnick, R. R. 1989, ApJ, 341, 1035
Schrijver, C. J., & Pols, O. R. 1993, A&A, 278, 51
Schröder, K.-P., Pols, O. R., & Eggleton, P. P. 1997, MNRAS, 285, 696
Spiegel, E. A. 1957, ApJ, 126, 202
Steffen, M. 1992, Habilitation thesis, Univ. Kiel
Stencel, R. E., Mullan, D. J., Linsky, J. L., Basri, G. S., & Worden, S. P. 1980, ApJS, 44, 383
Stępień, K., & Ulmschneider, P. 1989, A&A, 216, 139
Strassmeier, K. G., Handler, G., Paunzen, E., & Rauth, M. 1994, A&A, 281, 855
Sutmann, G., & Cuntz, M. 1995, ApJ, 442, L61
Sutmann, G., & Ulmschneider, P. 1995a, A&A, 294, 232
———. 1995b, A&A, 294, 241
Theurer, J., Ulmschneider, P., & Cuntz, M. 1997, A&A, 324, 587
Ulmschneider, P. 1970, Sol. Phys., 12, 403
———. 1986, A&A, 168, 308

Ulmschneider, P. 1988, A&A, 197, 223
———. 1989, A&A, 222, 171
———. 1990, in ASP Conf. Proc. 9, Cool Stars, Stellar Systems and the Sun, Proc. Sixth Cambridge Workshop, ed. G. Wallerstein (San Francisco: ASP), 3
———. 1991, in Mechanisms of Chromospheric and Coronal Heating, ed. P. Ulmschneider et al. (Berlin: Springer), 328
———. 1993, in Physics of Solar and Stellar Coronae, ed. J. L. Linsky & S. Serio (Dordrecht: Kluwer), 533
———. 1994, A&A, 288, 1021
Ulmschneider, P., Kalkofen, W., Nowak, T., & Bohn, H. U. 1977, A&A, 54, 61
Ulmschneider, P., Muchmore, D., & Kalkofen, W. 1987, A&A, 177, 292
Ulmschneider, P., Schmitz, F., Kalkofen, W., & Bohn, H. U. 1978, A&A, 70, 487
Ulmschneider, P., Theurer, J., & Musielak, Z. E. 1996, A&A, 315, 212
Vernazza, J. E., Avrett, E. H., & Loeser, R. 1981, ApJS, 45, 635
Vaiana, G. S., et al. 1981, ApJ, 244, 163
Walter, F. M., & Schrijver, C. J. 1987, in Cool Stars, Stellar Systems, and the Sun, Proc. Fifth Cambridge Workshop, ed. J. L. Linsky & R. E. Stencel (Berlin: Springer), 262
Zhugzhda, Y. D., Dzhalilov, N. S., & Staude, J. 1993, A&A, 278, L9